Route network design in low-altitude airspace for future urban air mobility operations: A case study of urban airspace of Singapore

Zhengyi Wang, Daniel Delahaye, Jean-Loup Farges, Sameer Alam

Route network design in low-altitude airspace for future urban air mobility operations

A case study of urban airspace of Singapore

(submitted to International Conference on Research in Air Transportation 2022)

Zhengyi Wang, Daniel Delahaye
Optim group
Ecole Nationale de l'Aviation Civile
Toulouse, France
{zhengyi.wang, daniel.delahaye}@enac.fr

Jean-Loup Farges
ONERA
Toulouse, France
jean-loup.farges@onera.fr

Sameer Alam
ATMRI
Nanyang Technological University
Singapore, Singapore
sameeralam@ntu.edu.sg

***Abstract*—The rapid growth of the metropolis leads to the proposal of alternative solutions, including the concept of Urban Air Mobility (UAM). Automated and highly-integrated UAM networks have been proved to have great advantages to handle UAM traffic flow with intense density and complexity in the near future. This research addresses designing UAM route networks in low-altitude airspace to minimize noise impact and maximize the efficiency and safety of UAM operations. Singapore's urban airspace is selected for the case study. On the basis of the open-source data of Singapore, the UAM network is designed as a grid-based multi-layer route network that supports two-way traffic. The topology features of the route network are analyzed. To provide alternative travel options for UAM traffic flow, we search for feasible routes between Origin-Destination (OD) pairs by solving k-Shortest Path with Diversity (KSPD) problem that minimizes link costs in terms of noise impact, safety and efficiency. The resulting feasible routes can potentially reduce airspace complexity and can be used for air traffic assignment. In addition, the impact of different parameter settings for link costs on UAM services is explored.**

***Keywords*—Urban Air Mobility, Route Network Design, Urban Airspace, Air Traffic Management**

1. Introduction

Urban Air Mobility (UAM) is an air transportation concept that supports passenger or cargo-carrying air transportation services in and around urban environments [1]. European Union Aviation Safety Agency (EASA) claimed that by 2024-25, UAM may be a lived reality in Europe [2]. To categorize the expected evolution stages of the UAM transportation system, NASA has developed a framework for UAM Maturity Levels (UML) [3]. During the intermediate and mature state of UML, the traffic density of UAM vehicles becomes intense. For high-density and complexity UAM operations in densely populated metropolitan areas, a centralized UAM transportation system with highly-integrated and automated route networks has great advantages [1, 4].

Significant progress has been made to design UAM route networks in urban airspace. FAA suggested adopting existing helicopter routes to construct route networks for early-stage UAM operations [1] . Tang et al. generated a 3D route network for all pairs of vertiports by using the visibility graph to avoid obstructions [5]. Some studies focus on UAM hub-and-spoke network design [6, 7]. Hong et al. designed a delivery network to support commercial stand-alone drone delivery service in an area with obstacles [8].

Many studies have only focused on on-demand transportation services. Since on-demand services are often represented by a fully-connected graph [7], the network size has to be limited in some studies. In addition, very few studies consider environmental impact in network design. The lack of integration with real-world data is also a shortcoming of some studies.

To fill the aforementioned research gap in UAM route network design and to minimize the impact on existing air traffic management systems, this paper proposes a methodology to design a UAM route network in low-altitude urban airspace in the presence of obstacles and hazardous airspace. Using a variety of open-source data, this approach is applied as a case study for parcel delivery services using Unmanned Aerial Vehicles (UAVs) as UAM vehicles in Singapore's urban airspace. Firstly, The UAM route network is designed as a grid-based network that avoids obstacles and airspace within which the aircraft is prohibited. Then, the link cost is defined in terms of noise impact on populations, airspace safety, and flight efficiency. Unlike most researches that only calculate the shortest path, we formulate a k-shortest path problem with diversity to select feasible routes between Origin-Destination (OD) pairs that minimize the route cost. The feasible routes with low similarity will provide more travel options, which can be used as pre-computed routes for traffic assignment models [9, 10] to support high-density and complexity flow-based operations.

2. Data source and data description

To model the static obstacles in the urban airspace of Singapore, we use ALOS World 3D-30m (AW3D30) data [11]. It is a global Digital Surface Model (DSM) that represents land terrain (natural and built features) with approximately a resolution of 30 meters. The ALOS World 3D data that covers Singapore is visualized in Figure 1.

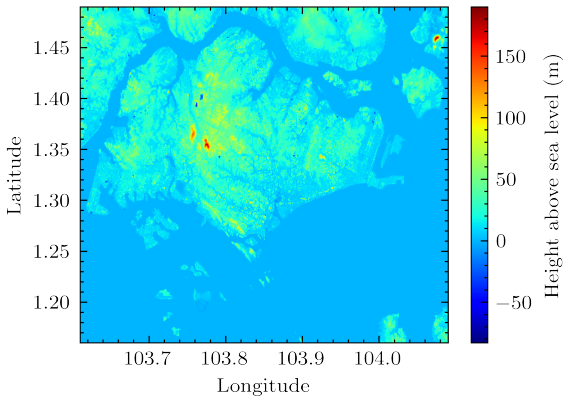

Figure 1: ALOS World 3D DSM data covering Singapore

To identify airspace that is potentially hazardous to UAM operations, the airspace classification information of Singapore [12] is used in this study. These airspace types are promulgated as follows [13, 14]:

- 5km of aerodromes: The airspace within 5km of the aerodrome area.
- Danger areas: The airspace within which activities dangerous to aircraft may exist at specified times.
- Prohibited areas: The airspace within which aircraft is prohibited, usually due to security purposes.
- Restricted areas: The airspace within which aircraft is restricted in accordance with certain specified conditions.
- Protected areas: The reserved airspace within which aircraft is not allowed for operation.

To sum up, prohibited and protected airspace are completely not allowed for UAM aircraft. All types of airspace are shown in Figure bounded by successive coordinates 2.

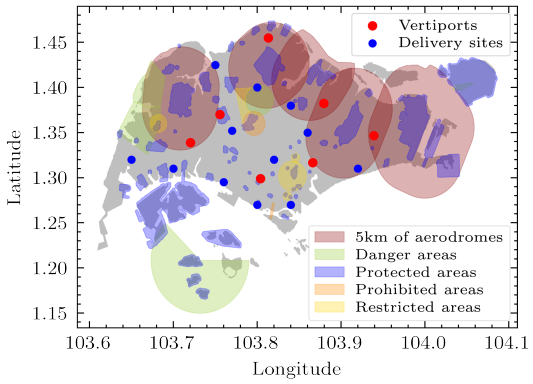

Figure 2: Singapore existing area limits for UAM flights

In addition, the location of vertiports is collected from a study that determined the optimal distribution of vertiports for Singapore considering both costs and society value [15]. Some locations of vertiports are modified to avoid hazardous airspace and terrain. Some delivery sites are randomly generated in the usable airspace. The location of vertiports and delivery sites are depicted in Figure 2.

To measure the noise impact of the UAM network on populations in different regions, the Singapore residents (as of June 2021) by planning area [16] and the boundary of planning area [17] data are collected. Singapore is divided into 332 subzones, and the total resident population in each subzone is illustrated in Figure 3. Note that in some subzones, the population may be nil or negligible.

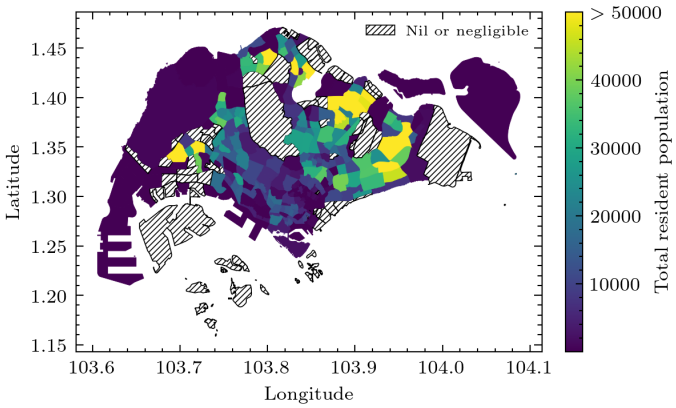

Figure 3: Total resident population of Singapore by subzone

3. Methodology

In the low-altitude urban airspace of a metropolitan area, the problem addressed here aims to design a multi-layer route network connecting Origin-Destination (OD) of UAM operations that optimizes the airspace usage, flight efficiency, and noise impact on residents, while keeping away from terrain and hazardous airspace. Based on the aforementioned datasets, we firstly determine the minimum spatial area to design the network and partition the area into grids. The grid points and air routes that have no interaction with the terrain and hazardous airspace are considered nodes and links, respectively. We search for the k-minimum cost path between each OD, where the link costs take into account airspace usage, noise impact, and flight efficiency.

A. Urban airspace usage and obstacles

According to the literature [18], several terms that describe the availability of airspace are firstly defined. The raw availability of urban airspace is represented by free airspace $\mathcal{A}_\mathrm{f}$, which is the airspace free of static obstacles Ω. Free airspace can be further divided into unusable airspace $\mathcal{A}_\mathrm{u}$ and usable airspace A_s. Unusable airspace includes prohibited areas, protected areas, and airspace affected by geofence associated with obstacles. The rest of the free airspace is denoted as usable airspace.

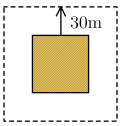

Figure 4: Geofence with keep-out distance of 30m

To avoid interfering with other air traffic, we create network layers on altitudes 150ft, 175ft, 200ft, 225ft, and 250ft. In different layers, we consider the terrain above the current altitude as static obstacles. To maintain safety separation between UAVs and obstacles, we apply geofence on terrain to impose geographical boundaries around the perimeter of obstacles as a virtual barrier. We define the minimum keep-out distance as d_k=30m in accordance with the specification of most countries, as illustrated in Figure 4.

B. Grid-based network

Firstly, World Geodetic System (WGS) is converted to Projected Coordinate System (PCS) EPSG:3414 for Singapore.

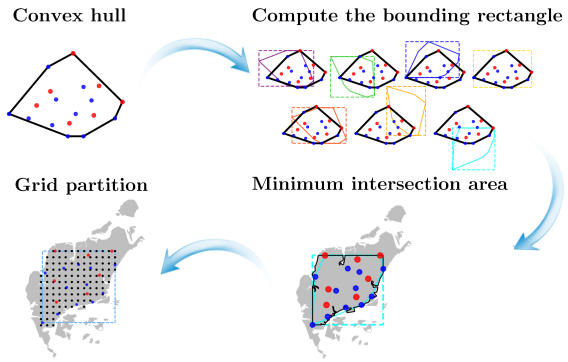

Figure 5: Calculation of minimum delivery area and grid-based discretization

To reduce the search space and the network construction cost, we calculate the Axis-aligned Minimum-Area Bounding Box (AMABB) of vertiports and delivery sites as the minimum spatial area to design route networks and discretize the space with waypoints. We use the method of rotating calipers [19] to calculate AMABB. The idea is to calculate the convex hull, then rotate by each edge orientation and compute the bounding rectangle. The minimum intersection area of the bounding rectangle and land of Singapore is the minimum area for delivery. Then, the area is discretized with grids starting from a corner point. To reduce the computation time while providing the right amount of node and link options, the size of discretization is set as d_g = 2000m. The diagram of these steps is illustrated in Figure 5.

The obstacles with geofence in the delivery area at different altitudes are shown in Figure 6. The urban airspace especially below 40m contains a large number of geographical constraints, which seriously limits the connections between nodes in the route network. This in turn causes bottlenecks of congestion, especially at intersections. which reduces overall airspace capacity and performance. As a remedy, the route network has a high level of flexibility and connectivity in the airspace at higher altitudes, where few or no static obstacles still exist.

At each altitude, the grid points that do not collide with obstacles, the points that have the same longitude and latitude as vertiports and delivery sites are selected as potential waypoints. Any pair of potential waypoints with a distance not greater than $\sqrt{2}d_g$ and not colliding with unusable airspace

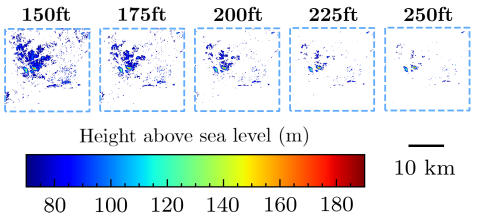

Figure 6: The distribution of obstacles with geofence in delivery area at altitude 150ft, 175ft, 200ft, 225ft, and 250ft

$\mathcal{A}_\mathrm{u}$ and obstacles Ω are connected as a link. In addition, the vertiports and delivery sites, and all waypoints directly above them are vertically connected as links. All these links form the set of link $\mathcal{E}$. All nodes that connect links in $\mathcal{E}$ form the set of node $\mathcal{V}$. The resulting route network is represented as $G = (\mathcal{E}, \mathcal{V})$.

C. Constraints and cost for feasible paths

To support high-density and complexity UAM traffic flow in route network G, the candidate paths $\mathcal{P} = \{\mathcal{P}_w | w \in \mathcal{W}\}$ should be determined for a given set of OD pair $\mathcal{W}$. We search for candidate paths that maximize flight safety and efficiency, minimize the noise impact on populations in the nearby subzones, and satisfy operational constraints in G.

The length of path d_p should not exceed the range of UAV, denoted as R_max:

$$d_p < R_\mathrm{max}, \quad p \in \mathcal{P} \tag{1}$$

The flight time should be limited to the endurance of UAV:

$$\sum_{e \in p} \frac{d_e}{s_e} < T_\mathrm{max}, \quad p \in \mathcal{P} \tag{2}$$

where s_e is the average speed of UAM traffic flow on link e. Note that, the maintenance and battery charging (or refueling) is assumed to be available both at vertiports and delivery sites. If not, the range and endurance of the UAV should be cut by half to consider the return trip.

It is noteworthy that some part of usable airspace may still be at risk, including aerodromes $\mathcal{A}_\mathrm{a}$, danger areas $\mathcal{A}_\mathrm{d}$, and prohibited areas $\mathcal{A}_\mathrm{p}$. The link traversing these areas is characterized by $\delta_{e,n}$ and penalized by a coefficient α_n, $n \in \{\mathrm{a}, \mathrm{d}, \mathrm{p}\}$. If link e traverse hazardous airspace n, $\delta_{e,n} = 1$, otherwise $\delta_{e,n} = 0$. According to the hazard level of airspace [13, 14], $\alpha_\mathrm{a}, \alpha_\mathrm{d}$, and α_p is set to be 0.2, 1, and 1, respectively. Then, we define the cost for crossing hazardous airspace $C_{\mathrm{o},e}$ for link $e \in \mathcal{E}$ based on the airspace type:

$$C_{\mathrm{h},e} = (\alpha_\mathrm{a}\delta_{e,\mathrm{a}} + \alpha_\mathrm{d}\delta_{e,\mathrm{d}} + \alpha_\mathrm{p}\delta_{e,\mathrm{p}}) \tag{3}$$

The cost of flight efficiency is calculated based on link length d_e and the type of link:

$$C_{\mathrm{f},e} = (\phi_\mathrm{h}\delta_{e,\mathrm{h}} + \phi_\mathrm{u}\delta_{e,\mathrm{u}} + \phi_\mathrm{d}\delta_{e,\mathrm{d}})d_e \tag{4}$$

where d_e is the length of link e, $\delta_{e,\mathrm{h}} = 1$ if link e is horizontal, otherwise 0. $\delta_{e,\mathrm{u}}$ and $\delta_{e,\mathrm{d}}$ similarly. $\phi_\mathrm{h}, \phi_\mathrm{u}, \phi_\mathrm{d}$ are efficiency coefficients for horizontal, upward and downward links, respectively. The coefficient is much larger for vertical

links than horizontal links because crossing altitudes will introduce traffic complexity in another dimension. The link for climbing is more penalized than the link for descent as it is more energy-consuming. Considering the distance gap between horizontal and vertical links, to make their costs of flight efficiency comparable, we set $\phi_{\mathrm{h}} = 0.005$, $\phi_{\mathrm{u}} = 1$ and ϕ_{d} = 0.5.

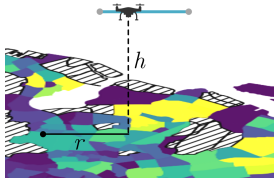

Figure 7: Measurement of SPL from UAV to a location

Another focus is to mitigate the noise impact of the designed link to populations in each subzone of Singapore. We use Sound Pressure level (SPL) to measure the pressure level of noise produced by UAVs [20]. We assume the UAV of height h produces the same reference noise of L_h at the ground point directly below, as shown in Figure 7. In addition, we denote the estimated UAV density on link e is N_e. Based on the inverse proportional law, the SPL L_r at the distance r from the point directly under UAV of density N_e can be simplified as:

$$L_r = L_h + 10\log_{10}\left(\frac{N_e h^2}{h^2 + r^2}\right) \tag{5}$$

The noise impact of the UAV traffic flow on a link e to a nearby subzone S can be represented as the integral of the SPL from a point distributed on the link to a point distributed in the subzone:

$$\hat{L}_e = \int_e f_e(b) \iint_S f_S(a) L_{\mathrm{dist}(a,b)} da db \tag{6}$$

where $\mathrm{dist}(a, b)$ is the euclidean distance between point a and b, $f_S(a)$ is the Probability Density Function (PDF) of a point a in polygon S, $f_e(b)$ is the PDF of a point b in line segment e. The details for calculating $\hat{L}_e$ is given in Appendix A.

We search for subzones with polygonal shapes in the vicinity of each link modeled as a line segment. The total noise impact from a link e to all nearby subzones is defined as:

$$C_{\mathrm{n},e} = \sum_{\mathrm{dist}(S,e) \le d_t} P_S \hat{L}_e \tag{7}$$

where P_S is the population in subzone S, d_t is the distance threshold. To avoid significant effects by other impact factors such as wind, d_t is set as a short distance 2000m. $\mathrm{dist}(S, e)$ is the distance from subzone S to link e and is defined as:

$$\mathrm{dist}(S, e) = \int_e f_e(b) \iint_S f_S(a)\mathrm{dist}(a, b) da db \tag{8}$$

The calculation of equation (8) is the same as equation (6). The total cost for a link e is given as:

$$C_e = w_{\mathrm{h}}\tilde{C}_{\mathrm{h},e} + w_{\mathrm{f}}\tilde{C}_{\mathrm{f},e} + w_{\mathrm{n}}\tilde{C}_{\mathrm{n},e}, \quad e \in \mathcal{E} \tag{9}$$

where $w_{\mathrm{h}}, w_{\mathrm{f}}, w_{\mathrm{n}}$ are weighting parameters between 0 and 1 and satisfy $w_{\mathrm{h}} + w_{\mathrm{f}} + w_{\mathrm{n}} = 1$, $\tilde{C}_{\mathrm{n},e}$, $\tilde{C}_{\mathrm{h},e}$,$\tilde{C}_{\mathrm{f},e}$ are normalized costs. The prior scaling of the objectives are mandatory to make them comparable. Min-max normalization is used in this study:

$$\tilde{C} = \frac{C - \min(C)}{\max(C) - \min(C)} \tag{10}$$

The path cost is the sum of the costs of links that belong to this path:

$$C_p = \sum_{e \in p} C_e \tag{11}$$

D. Finding k-shortest path

For a route network $\mathcal{G}$ in a metropolitan area, the number of paths connecting each OD pair may be very large. To reduce the computational burden and potentially decrease the airspace complexity, a natural idea is to reduce the number of candidate paths between each OD pair by searching the k-Shortest Paths (KSP) based on the path cost defined previously. Denote the acyclic paths satisfying constraints (1-2) as $\hat{\mathcal{P}}$, then the problem is to find for each OD w the set of k paths $\mathcal{P}_w$ satisfying $\forall p \in \hat{\mathcal{P}}/\mathcal{P}_w$, $\forall q \in \mathcal{P}_w$, $C_p \ge C_q$.

However, in KSP problems, it is very likely that some of the shortest paths are highly similar. They share a large part of sub-paths, and the resulting paths provide low flexibility and few alternatives for air traffic assignment. To this end, we search k-Shortest Paths with Diversity (KSPD). Since KSPD has been proved to be NP-hard [21], we use a greedy algorithm to approximate the KSPD problem. A similarity metric is defined as follows:

$$\mathrm{sim}(p, q) = \frac{C_{\mathcal{E}_p \cap \mathcal{E}_q}}{2C_p} + \frac{C_{\mathcal{E}_p \cup \mathcal{E}_q}}{2C_q} \tag{12}$$

where $\mathcal{E}_p$ is the set of links on path p.

If the similarity between two paths is higher than a threshold, they are considered similar paths and cannot exist at the same time. The pseudocode of this algorithm is given in Algorithm 1. The idea is to insert the next shortest path that is sufficiently dissimilar to all shortest paths in the result set. This algorithm has been shown to have a high approximation ratio to the exact solution in real-world applications [21]. The similarity threshold τ_{p} is chosen to be 0.6.

4. Result and Discussion

A. Experiment setting

According to acoustical measurement data of UAV in [22], we roughly set $L_{150\mathrm{ft}}$ = 80dB, $L_{175\mathrm{ft}}$ = 78dB, $L_{200\mathrm{ft}}$ = 76dB, $L_{225\mathrm{ft}}$ = 74dB, and $L_{250\mathrm{ft}}$ = 72dB. Referring to [23], the range and endurance of UAV are set as $R_{\max}$ = 25km and $T_{\max}$ = 1h. The average speed of UAM traffic flow on horizontal links and vertical links are set to be 15m/s and 2m/s. For each OD pairs, we select the number of shortest paths $k = 20$, and the estimated density of UAV on all links is the same. The framework is implemented in Python 3.7 on a laptop with Intel i7-8750H CPU and 32GB DDR4 RAM.

Algorithm 1 Greedy algorithm for KSPD problem

Input: Air transport network: G, OD pairs: $\mathcal{W}$, similarity function: $\mathrm{sim}(\cdot,\cdot)$, number of shortest path: k, and similarity threshold: τ_{p}

Output: k-shortest path for OD pairs: Ψ

procedure KSPD
  for $w \in \mathcal{W}$ **do**
    $\hat{\mathcal{P}} \leftarrow$ Set of acyclic paths that connects OD pair w and satisfies the constraint (1-2)
    $p^* \leftarrow \arg\min_{p\in\hat{\mathcal{P}}} C_p$
    $\hat{\mathcal{P}} \leftarrow \hat{\mathcal{P}}/\{p^*\}$
    $\Psi_w \leftarrow \{p^*\}$
    while $|\Psi_w| < k$ and $|\hat{\mathcal{P}}| > 0$ **do**
      $p^* \leftarrow \arg\min_{p\in\hat{\mathcal{P}}} C_p$
      $\hat{\mathcal{P}} \leftarrow \hat{\mathcal{P}}/\{p^*\}$
      if $\forall p \in \Psi_w, \mathrm{sim}(p,p^*) < \tau_{\mathrm{p}}$ **then**
        $\Psi_w \leftarrow \Psi_w \cup \{p^*\}$
      end if
    end while
  end for
  $\Psi \leftarrow \{\Psi_w | w \in \mathcal{W}\}$
  return Ψ
end procedure

B. Route network

The resulting multi-layer route network is shown in Figure 8. The vertiports, delivery sites, and waypoints are marked in the figure. The links in different altitude layers are marked in different colors. The resulting route network contains 5 altitude layers. To compare the horizontal network in different altitude layers, by removing vertical connections, some basic topology features are calculated on the basis of network theory. These topology features include the number of nodes, number of links, average degree, average clustering coefficient [24], and degree of assortativity [25]. Their values for different altitude layers are summarized in Table I.

As is shown in Table I, the network has more number of nodes and links at higher altitudes, because higher altitude layers have fewer obstacles. The result of the average degree indicates that each node has more connections to neighbors as altitude increases. The growth of the average clustering coefficient with altitude signifies that nodes tend to cluster together as altitude increases. Except for altitude layer 150ft which is non-assortative, the degree of assortativity for other network layers is positive, which means that high degree nodes are more likely to attach to high degree nodes, that is, these networks are assortative.

C. Link costs

The normalized link cost for crossing hazardous airspace $\tilde{C}_{\mathrm{h},e}$, of flight efficiency $\tilde{C}_{\mathrm{f},e}$, and of noise impact $\tilde{C}_{\mathrm{n},e}$ are calculated and represented in Figure 9, 10, and 11, respectively.

According to Figure 2, since hazardous airspace occupies a large amount of Singapore's airspace, most of the links

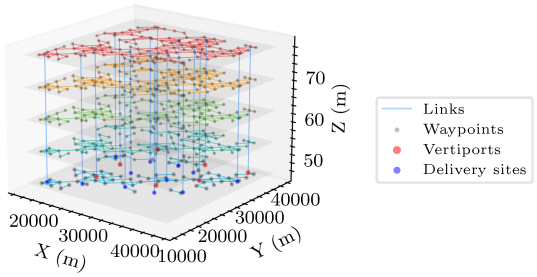

Figure 8: The resulting multi-layer route network in Singapore urban airspace

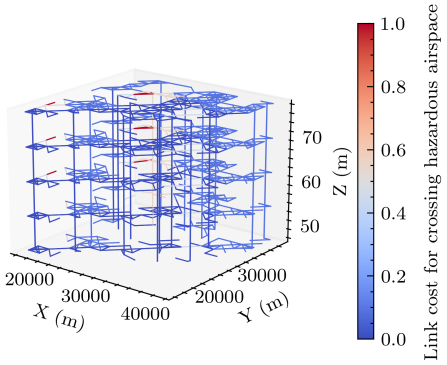

Figure 9: Normalized link cost for crossing hazardous airspace in route network

in the route network have to traverse hazardous airspace. This fact is consistent with Figure 9. Nevertheless, airspace within 5km of aerodromes takes up the largest proportion of hazardous airspace, so most links have a low cost for traversing hazardous airspace. There are some areas where different types of hazardous airspace overlap, where link costs are significant.

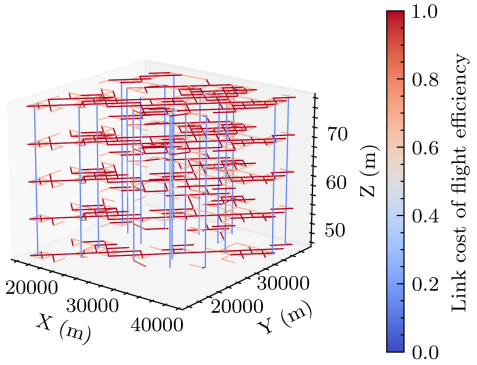

Figure 10: Normalized link cost of flight efficiency in route network

In terms of link cost of flight efficiency shown in 10, for horizontal links, longer links are less efficient and have higher costs. Though vertical links are heavily penalized, it can be seen that the costs of flight efficiency for vertical links are still less than for horizontal links. Note that, the flight efficiency costs for upward links are two times larger than downward links.

In Figure 11, links with high cost of noise impact are calculated. Referring to Figure 3, they are mainly distributed around densely populated areas.

TABLE I: Basic topology features of different altitude layers and the whole route network

Network	Number of nodes	Number of links	Average degree	Average clustering coefficient	Degree of assortativity
Network layer at 150ft	75	216	5.7600	0.3138	-0.0004
Network layer at 175ft	102	336	6.5882	0.3875	0.3613
Network layer at 200ft	111	444	8.0000	0.4709	0.2139
Network layer at 225ft	115	524	9.1130	0.5081	0.2775
Network layer at 250ft	115	546	9.4957	0.5154	0.3383
The whole route network	529	2218	8.3856	0.3789	0.3789

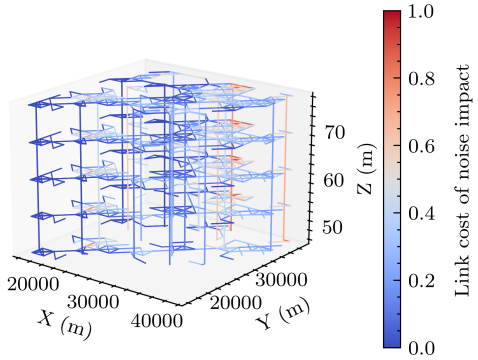

Figure 11: Normalized link cost of noise impact in route network

D. Feasible path between OD pairs

To compare the relative importance of three types of link cost, in equation (9), the different combination of weighting parameters are examined. The weighting parameters $w_{\mathrm{h}}, w_{\mathrm{f}}, w_{\mathrm{n}}$ are set to be [1/3, 1/3, 1/3], [2/3, 1/6, 1/6], [1/6, 2/3, 1/6], and [1/6, 1/6, 2/3]. In these four cases, the first parameter setting treats all link costs as equivalent. Other cases consider that one of the link costs is more important than the other link costs.

As the previous steps can be performed offline, we focus on the computation time of feasible path generation. These four route networks cost 11.19s, 11.74s, 13.39s and 11.31s, respectively. In addition, the average cost for k-shortest paths between OD pairs is shown in Figure 12. The coordinates indicate the index of vertiports and delivery sites. For OD pairs involving some vertiports, such as the vertiports 0, 1, 2, 3, the average path cost for different weighting parameters remains low. The reason is that they are more accessible to most delivery sites through the UAM route network. On the contrary, the average path costs for OD pairs that involve vertiport 4, 5, 6 are always at a high level. In Figure 12b, the link cost for crossing hazardous airspace is considered more important. In this case, the peak value of average path cost is the lowest among the four cases, because most hazardous airspace is covered by aerodromes, which is less penalized. Figure 12c corresponds to the case in which the link cost of flight efficiency is more important. The pattern of average path cost in this case is similar to the first case (Figure 12a), but the peak value is much higher. This fact indicates that feasible paths between some OD pairs are less efficient, such as OD pairs in the lower left part of Figure 12c. In the last case, it can be seen from Figure 12d that paths connecting vertiport 4 have significant costs. The reason lies in the fact that vertiport 4 is located in a densely populated downtown area.

To visualize the shortest path in the network representation, Figure 13 illustrate the number of times that each link appears in the k-shortest paths given different weighting parameters. A link is removed from the network if none of the feasible paths pass through it. At a quick glance, all altitude layers in these four networks are utilized. Vertical links, as the connection of adjacent altitude layers, appear most in the route network. According to different weighting parameters, the route network is created by minimizing the criteria formulized in equation (11). Slight differences including link counts and network topology can be observed in these networks. To sum up, the resulting UAM route network provides many travel alternatives, which can be used by air traffic flow management and air traffic assignment to mitigate the complexity and congestion of airspace.

5. Conclusion and Perspectives

The methodology proposed in this paper aims to define a set of alternative routes in a UAM context. Based on various data and grid networks, relevant constraints and costs are considered to search for k-shortest paths with diversity. The feasibility of this approach is demonstrated by its application to a parcel delivery service for Singapore.

In future work, it would be interesting to estimate the density of operations and analyze the impact of bottlenecks using different network structures. Another important extension of the work could consist in considering mixed traffic, for instance, automated air taxis sharing the airspace with parcel delivery UAVs. In addition, future studies could investigate the complete information processing chain by integrating the methodology proposed here with an air traffic assignment method using the sets of paths resulting from the solution to the KSPD problem.

Acknowledgement

This work is partially supported by the research project CONCORDE of the Defense Innovation Agency (AID) of the French Ministry of Defense (20196500900047075O1).

References

[1] Federal Aviation Administration (FAA), "Urban Air Mobility (UAM) concepts of operations v1.0," U.S. department of transportation, Tech. Rep., 2020.

[2] European Union Aviation Safety Agency (EASA), "Study on the societal acceptance of urban air mobility in europe," 2021, (visited 10/02/2022). [Online]. Available: https://www.easa.europa.eu/downloads/127760/en

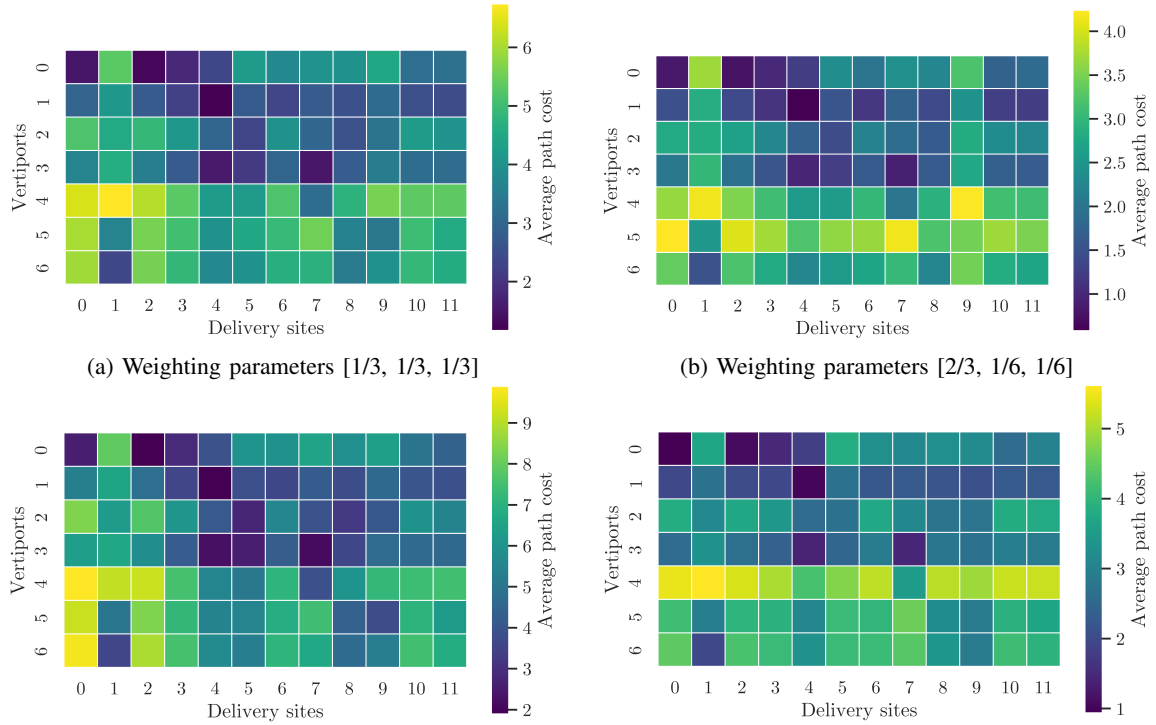

(a) Weighting parameters [1/3, 1/3, 1/3]

(b) Weighting parameters [2/3, 1/6, 1/6]

(c) Weighting parameters [1/6, 2/3, 1/6]

(d) Weighting parameters [1/6, 1/6, 2/3]

Figure 12: Average path cost for different OD pair with different weighting parameters

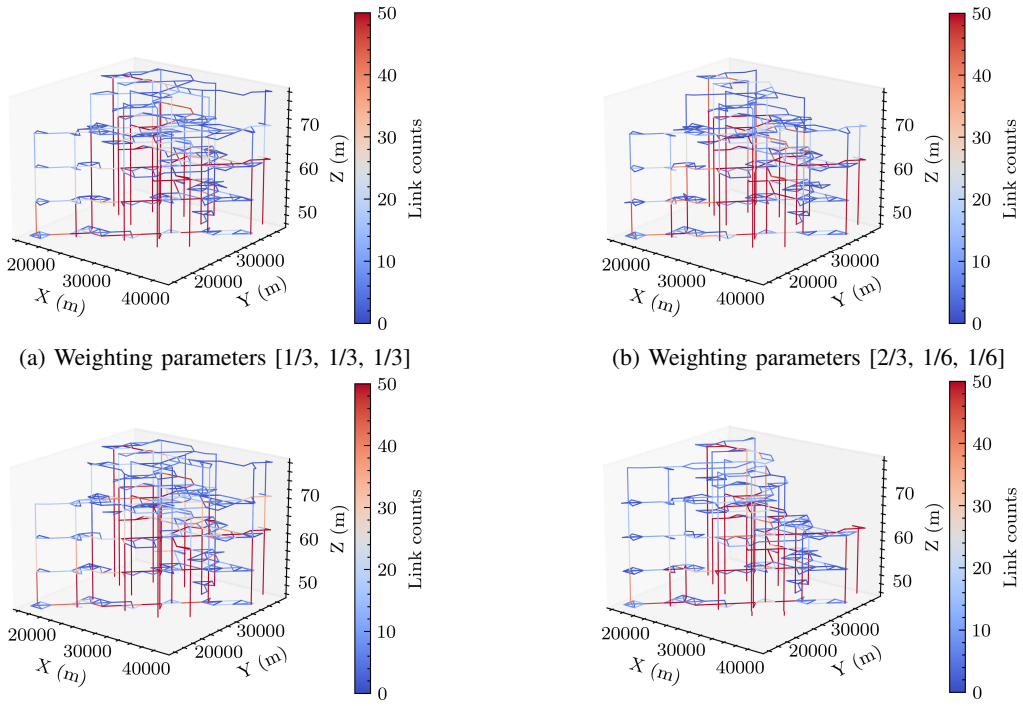

(a) Weighting parameters [1/3, 1/3, 1/3]

(b) Weighting parameters [2/3, 1/6, 1/6]

(c) Weighting parameters [1/6, 2/3, 1/6]

(d) Weighting parameters [1/6, 1/6, 2/3]

Figure 13: The number of times the links appear in the k-shortest paths between OD pairs with different weighting parameters

[3] K. H. Goodrich and C. R. Theodore, "Description of the nasa urban air mobility maturity level (uml) scale," in *AIAA Scitech 2021 Forum*, 2021, p. 1627.

[4] K. H. Goodrich and B. Barmore, "Exploratory analysis of the

airspace throughput and sensitivities of an urban air mobility system," in *2018 Aviation Technology, Integration, and Operations Conference*, 2018, p. 3364.
[5] H. Tang, Y. Zhang, V. Mohmoodian *et al.*, "Automated flight planning of high-density urban air mobility," *Transportation Research Part C: Emerging Technologies*, vol. 131, p. 103324, 2021.
[6] Z. Wu and Y. Zhang, "Integrated network design and demand forecast for on-demand urban air mobility," *Engineering*, vol. 7, no. 4, pp. 473–487, 2021.
[7] L. C. Willey and J. L. Salmon, "A method for urban air mobility network design using hub location and subgraph isomorphism," *Transportation Research Part C: Emerging Technologies*, vol. 125, p. 102997, 2021.
[8] I. Hong, M. Kuby, and A. T. Murray, "A range-restricted recharging station coverage model for drone delivery service planning," *Transportation Research Part C: Emerging Technologies*, vol. 90, pp. 198–212, 2018.
[9] S. C. Dafermos and F. T. Sparrow, "The traffic assignment problem for a general network," *Journal of Research of the National Bureau of Standards B*, vol. 73, no. 2, pp. 91–118, 1969.
[10] Z. Wang, D. Delahaye, J.-L. Farges *et al.*, "Air traffic assignment for intensive urban air mobility operations," *Journal of Aerospace Information Systems*, vol. 18, no. 11, pp. 860–875, 2021.
[11] "Alos global digital surface model "alos world 3d - 30m (aw3d30)" (version 3.2)," 2022, (visited 10/02/2022). [Online]. Available: https://www.eorc.jaxa.jp/ALOS/en/dataset/aw3d30
[12] "Airspace classification information of singapore," 2022, (visited 10/02/2022). [Online]. Available: https://www.onemap.gov.sg/main/v2/dronequery
[13] Civil Aviation Authority of Singapore, "Air Navigation (Protected Areas) (No. 2) Order," 2015, (version in force from 17/07/2015). [Online]. Available: https://www.caas.gov.sg/docs/default-source/pdf
[14] ——, "Air navigation regulations (101 - unmanned aircraft operations)," 2019, (version in force from 13/11/2021). [Online]. Available: https://www.caas.gov.sg/docs/default-source/docs---legal/air-navigation-(101-unmanned-aircraft-unmanned-aircraft-operations)-regulations-2019.pdf
[15] Y. Zeng, K. H. Low, M. Schultz *et al.*, "Future demand and optimum distribution of droneports," in *2020 IEEE 23rd International Conference on Intelligent Transportation Systems (ITSC)*. IEEE, 2020, pp. 1–6.
[16] "Singapore residents by planning area / subzone, age group, sex and type of dwelling," 2021, (visited 10/02/2022). [Online]. Available: https://www.singstat.gov.sg/find-data/search-by-theme/population/geographic-distribution/latest-data
[17] "Master plan subzone boundary (no sea)," 2019, (visited 10/02/2022). [Online]. Available: https://data.gov.sg/dataset
[18] J. Cho and Y. Yoon, "How to assess the capacity of urban airspace: A topological approach using keep-in and keep-out geofence," *Transportation Research Part C: Emerging Technologies*, vol. 92, pp. 137–149, 2018.
[19] G. T. Toussaint, "Solving geometric problems with the rotating calipers," in *Proc. IEEE Melecon*, vol. 83, 1983, p. A10.
[20] G. Scozzaro, D. Delahaye, and A. Vela, "Noise abatement trajectories for a uav delivery fleet," in *SID 2019, 9th SESAR Innovation Days*, 2019.
[21] H. Liu, C. Jin, B. Yang *et al.*, "Finding top-k shortest paths with diversity," *IEEE Transactions on Knowledge and Data Engineering*, vol. 30, no. 3, pp. 488–502, 2017.
[22] B. Schäffer, R. Pieren, K. Heutschi *et al.*, "Drone noise emission characteristics and noise effects on humans—a systematic review," *International Journal of Environmental Research and Public Health*, vol. 18, no. 11, p. 5940, 2021.
[23] A. Troudi, S.-A. Addouche, S. Dellagi *et al.*, "Sizing of the drone delivery fleet considering energy autonomy," *Sustainability*, vol. 10, no. 9, p. 3344, 2018.
[24] J. Saramäki, M. Kivelä, J.-P. Onnela *et al.*, "Generalizations of the clustering coefficient to weighted complex networks," *Physical Review E*, vol. 75, no. 2, p. 027105, 2007.
[25] M. E. Newman, "Mixing patterns in networks," *Physical review E*, vol. 67, no. 2, p. 026126, 2003.
[26] U.S. Census Bureau, *Geographic Areas Reference Manual*. U.S. Department of Commerce, Economics and Statistics Administration, Bureau of the Census, 1994.
[27] W. Mu and D. Tong, "Distance in spatial analysis: measurement, bias, and alternatives," *Geographical Analysis*, vol. 52, no. 4, pp. 511–536, 2020.
[28] ——, "Computation of the distance between a polygon and a point in spatial analysis," *International Journal of Geographical Information Science*, pp. 1–26, 2021.

APPENDIX

A. Exact expression of noise impact from a link to a polygon

Assuming that individuals are uniformly distributed in a polygon and there is a uniform traffic flow of UAV on each link, then $f_S(a) = 1/|S|$ and $f_e(b) = 1/d_e$, where $|S|$ is the area of polygon and d_e is the length of line segment e. $\hat{L}_e$ can be simplified as:

$$\hat{L}_e = \frac{1}{|S|d_e} \int_e \iint_S L_{\mathrm{dist}(a,b)} dadb \tag{13}$$

As stated by [26], many geographic regions including census tracts, block groups, and blocks are largely delineated by streets and are close to the rectangle in shape. To efficiently calculate the multiple integrals in L_e, the subzone can be approximated by an AMABB [27, 28]. The route network is rotated by θ according to the reference point of AMABB, where θ is the angle by which the Minimum Bounding Box (MBB) rotates to become an AMABB.

After the rotation, the notation for calculating the noise metric of horizontal links and vertical links is given in Figure A.1. We give the exact expression of noise impact from a link to the nearby subzones:

If the link is vertical, which corresponds to Figure A.1b,

$$\hat{L}_e = \int_{h_{\min}}^{h_{\max}} \int_{x_{\min}}^{x_{\max}} \int_{y_{\min}}^{y_{\max}} L_h + 10\log_{10}\left(\frac{h^2}{h^2+(x-x_0)^2+(y-y_0)^2}\right) dhdxdy \tag{14}$$

If the link is horizontal (corresponds to Figure A.1a) and the x-coordinates of both endpoints are different,

$$\hat{L}_e = \int_{\min(x_0,x_1)}^{\max(x_0,x_1)} \int_{x_{\min}}^{x_{\max}} \int_{y_{\min}}^{y_{\max}} L_h + 10\log_{10}\left(\frac{h^2}{h^2+(x-u)^2+(y-\frac{(u-x_0)(y_1-y_0)}{x_1-x_0}-y_0)^2}\right) dudxdy \tag{15}$$

If the link is horizontal and the x-coordinates of both endpoints are the same,

$$\hat{L}_e = \int_{\min(y_0,y_1)}^{\max(y_0,y_1)} \int_{x_{\min}}^{x_{\max}} \int_{y_{\min}}^{y_{\max}} L_h + 10\log_{10}\left(\frac{h^2}{h^2+(x-x_0)^2+(y-v)^2}\right) dvdxdy \tag{16}$$

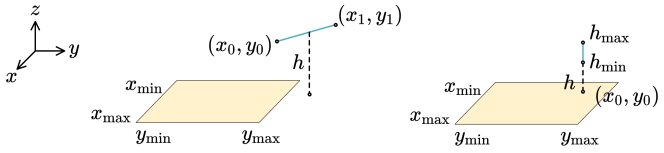

(a) Horizontal link (b) Vertical link

Figure A.1: Notation for different type of links

Numerical integration method is used to solve these integrals.